Electron-impact ionization of Xe^{24+} ions: Theory versus experiment

Pengfei Liu,[1] Jiaolong Zeng,[1,2] Alexander Borovik, Jr.,[3] Stefan Schippers,[3] and Alfred Müller[3]

[1]*Department of Physics, College of Science, National University of Defense Technology, Changsha Hunan 410073, People's Republic of China*

[2]*IFSA Collaborative Innovation Center, Shanghai Jiao Tong University, Shanghai 200240, People's Republic of China*

[3]*Institut für Atom und Molekülphysik, Justus-Liebig-Universität Giessen, D-35392 Giessen, Germany*

(Received 6 May 2015; published 6 July 2015)

Absolute and energy-scanned electron-impact ionization cross sections of Xe^{24+} ions in their ground level have been measured by employing a crossed-beams technique in the collision energy range from below threshold to 1000 eV. Direct ionization and excitation-autoionization cross sections were calculated using a detailed level-to-level distorted-wave method. Large discrepancy between the theoretical result, only including these two processes, shows the importance of additional ionization channels via resonant-excitation double autoionization (REDA). The carefully investigated convergence trend of REDA processes with the principal and angular-momentum quantum numbers of the recombined electron, n' and l', respectively, shows that sufficiently large n' and l' have to be included in the calculation of the total REDA contribution to correctly interpret the experiment.

DOI: 10.1103/PhysRevA.92.012701 PACS number(s): 34.80.Dp, 32.80.Hd

I. INTRODUCTION

Electron-impact ionization is among the most important atomic processes in hot plasmas and is a subject of continued interest. Accurate determination of ionization cross sections is important in modeling both astrophysical and laboratory plasmas [1,2]. The cross sections are needed to determine the charge-state distribution, the effective charge, power balance, impurity composition, and to infer the physical conditions of plasmas such as the electron temperature, electron density, and elemental abundance [3,4].

The ongoing interest in electron-impact ionization is well reflected in the investigation of xenon ions. Over the past decades, a substantial number of experimental studies were carried out to obtain electron-impact ionization cross sections of low-charge Xe^{q+} ($q \leqslant 10$) [5–24]. The detailed information about literature for specific ions is summarized in a recent publication by Borovik *et al.* [24]. More recently, such experimental studies were extended to moderately charged Xe^{q+}(q = 10–17) [25,26]. For higher charge states of Xe^{q+} ($q \geqslant 18$), however, few experimental investigations are found in the literature [27]. To the best of our knowledge, highly charged ions with q = 43–48 were experimentally produced through electron-impact ionization and excitation in an electron-beam ion trap [28], however, no absolute cross sections were reported. In this work, we present absolute and energy-scanned cross sections for the electron-impact ionization of highly charged Xe^{24+} along with detailed level-by-level theoretical calculations. The measurements comprise detailed data for the most highly charged ion ever addressed in electron-ion crossed-beams experiments.

Past experimental and theoretical studies show that the direct ionization (DI) and excitation-autoionization (EA) processes dominate the total cross section for the low-charge xenon ions ($q \leqslant 10$). Detailed energy-scan data for these ions show, however, that measurable contributions due to resonant-excitation double-autoionization (REDA) processes [2] occur for all xenon ion charge states with $q \geqslant 2$ [24,27]. With the increase of the ionization stage to moderately charged ions ($10 \leqslant q \leqslant 17$), REDA processes start to play a more significant role [25,26]. For higher ionization stages with $q > 18$, REDA processes have turned out to provide a significant contribution to the electron-impact ionization cross section. However, detailed level-to-level calculations of the REDA processes are extremely time-consuming because a large number of levels have to be included to obtain a converged result.

The detailed calculation of the cross section arising from REDA processes involves complex Auger and radiative decay pathways. Accurately determining all relevant pathways and their branching ratios (BR) for many-electron heavy ions is a troublesome task. Few calculations have been carried out including REDA in the theoretical investigation of electron-impact ionization of ions and are restricted to cases with relatively few active electrons. The REDA process was predicted by LaGattuta and Hahn [29] and experimentally verified for the first time by Müller *et al.* [30,31]. Early theoretical work on REDA was reviewed by Moores and Chen [32]. Only few theoretical treatments were reported thereafter. Examples are calculations for Li-like [33–35] and Na-like ions [36–38] and, more recently, for He-like N^{5+} [39] and Rb-like Sn^{13+} ions [40,41].

For Xe^{24+}, the only two theoretical studies available in the literature [42,43] show that the ionization cross section is still dominated by the indirect EA processes, in particular near the ionization threshold. Mitnik *et al.* [43] calculated detailed EA contributions to ionization cross sections using a relativistic distorted-wave method for Zn-like ions ($34 \leqslant Z \leqslant 92$) including Xe^{24+}. EA processes to $3d^9 4s^2 nl$ (n = 4–7) and $3p^5 3d^{10} 4s^2 nl$ (n = 4,5) are included in their calculations. Pindzola *et al.* [42] carried out configuration-average distorted-wave calculations considering excitations from the $3s$, $3p$, and $3d$ subshells to nl up to Rydberg states $6f$ for an initial $3s$ or $3p$ electron, and up to $8g$ for an initial $3d$ electron. They evaluated the REDA contributions to the ionization cross section by using the level-resolved R-matrix method [44]. They wrote in their publication [42]: "Since the resonant-capture double-autoionization contributions for all transitions, as calculated using the R-matrix method, were found to be quite small, they were not included in the total cross sections."

In the present work, we investigate the electron-impact ionization cross section of Xe^{24+} both experimentally and theoretically. The measurements have been performed

employing a crossed-beams technique. Absolute cross sections of Xe^{24+} and a high-precision energy-scan spectrum providing details of the cross section function were obtained. To understand the roles of DI, EA, and REDA processes, we carried out detailed level-to-level calculations by using a distorted-wave approximation. New features different from the results reported previously for xenon ions in lower charge states are discussed in detail.

The paper is organized as follows. Section II provides an overview of the experimental setup and procedures. It focuses on the specific issues associated with the present measurements. Section III describes the main theoretical concepts including aspects specific to electron-impact ionization of Xe^{24+}. Section IV details the cross-section contributions from excited levels and investigates their convergence with increasing principal and orbital momentum quantum numbers. Theoretical and experimental cross sections are compared to one another and to previous calculations. Conclusions are drawn in Sec. V.

II. EXPERIMENT

The experimental data on electron-impact single ionization of Xe^{24+} have been obtained by using the most recent electron-ion crossed-beams setup at Giessen University. Absolute cross sections were measured by employing the well-established animated-beam technique [45–47]. In addition, a high-resolution energy-scan technique was used to detect fine details in the energy dependence of the measured cross sections [30,31,48]. The experimental arrangement and procedures have been previously discussed by Jacobi *et al.* [49] and Borovik Jr. *et al.* [50]. Referring to these publications, only a brief overview is provided here together with details concerning the present experiment.

The primary Xe^{24+} ions were produced in a 10-GHz all-permanent-magnet electron-cyclotron-resonance (ECR) ion source [51]. A mixture of xenon and oxygen gas was fed into the plasma chamber via two identical leak valves. The proportion of the gas flows and the total pressure in the source together with exceptionally fine adjustments of other ion source parameters appeared to be key factors for producing Xe^{24+} ion beams with intensities suitable for performing the experiment. The total pressure of the xenon-oxygen mixture was 2.4×10^{-4}mbar measured in the gas-inlet section. The relative composition of this mixture was optimized for maximum output of Xe^{24+} ions but was not measured. However, the settings of the two leak valves suggest less than 5% of xenon and over 95% of oxygen.

After extraction and acceleration with a voltage of 12 kV, the ions were directed into a dipole analyzing magnet with 90° deflection and an isotopically pure $^{132}Xe^{24+}$ ion beam was thus produced. Before entering the interaction region, the ion beam was charge-state purified once again by passing a 90° spherical deflector and collimated by two pairs of four-jaw slits separated from one another by about 18 cm. In order to ensure the complete transmission of both the parent ion beam to the final Faraday cup and the product ions to the single-particle detector the primary ion beam was collimated to the size of 0.7×0.7 mm^2 during the measurements of absolute single-ionization cross sections. For energy scans, the collimation conditions could be relaxed and the size of the ion beam was increased to 1.0×1.0 mm^2. The resulting ion beam currents employed in the experiments were 1.3 and 5.3 nA for the absolute cross-section and energy-scan measurements, respectively.

In the interaction region the beam of $^{132}Xe^{24+}$ ions was crossed by an intense ribbon-shaped electron beam produced by a high-current electron gun [52]. The space-charge limited intensity of the electron beam varied as a function of energy and reached a maximum value of 450 mA at 1000 eV. At energies beyond 1000 eV the operation of the gun becomes unstable. For an extension of the energy range accessible in electron-ion collision experiments a new electron gun has been designed and built [53,54] which will be used in the crossed-beams setup in the near future.

The product Xe^{25+} ions resulting from ionizing electron-ion collisions were separated from the primary Xe^{24+} ion beam by a second 90° bending magnet, identical to the first magnetic analyzer. After passing an electrostatic spherical 180° out-of-plane deflector, the product ions were registered by a high-efficiency single-particle detector [55,56]. For the measurement of the primary-ion beam current two movable Faraday cups are installed in the vacuum chamber of the second analyzer magnet. The layout of the electron-ion crossed-beams setup (see [49]) allows one to collect all Z^{q+} parent ions in one of these Faraday cups, when appropriately positioned according to the primary ion charge state q, and to register all $Z^{(q+1)+}$ single-ionization product ions in the detector simultaneously as long as $q < 18$. In the present case the product Xe^{25+} and primary Xe^{24+} ion beams could not be sufficiently separated from one another for complete collection of the primary ion beam without having the product beam intercepted by the housing of the Faraday cup. Therefore, primary-ion beam-current measurements were performed separately before and after each cross-section measurement for which the product ions were recorded by the detector electronics for a certain time span. Considering the high stability of the ion beam this introduced little additional uncertainty of the resulting absolute cross sections.

The calculation of the cross sections on the basis of the measured raw data as well as the evaluation of the error budget have been discussed in detail by Rausch *et al.* [57]. The total systematic uncertainty of the absolute cross-section determination was obtained as the quadrature sum of the systematic uncertainties of the experimentally measured parameters entering the cross-section evaluation. In the electron energy range from 450 to 1000 eV the total uncertainty was found to be 8.3% including negligible statistical uncertainties [57]. In the present experiment three additional sources of uncertainty have to be considered: (i) With the relatively low ionization cross section of Xe^{24+} and low parent-ion particle flux (with 1.3 nA of electrical current, this was only about 3.4×10^8 s^{-1}) the statistical uncertainties were larger than usual; (ii) the fact that the primary ion current could not be measured simultaneously with the signal counts, introduced additional uncertainty; (iii) subtraction of a relatively strong background cross section that was found to contribute to the total ionization signal caused a substantial increase of the overall uncertainty.

On the basis of experiences gained with the measurements on electron-impact ionization of N^{5+} ions [39] we attribute the

observed background to the presence of a very small fraction of parent ions in high Rydberg states with principal quantum numbers n sufficiently high to provide lifetimes comparable to or greater than the flight times of the ions from the ECR source to the electron-ion interaction region but sufficiently low to evade field ionization in the motional electric field seen by the ions inside the analyzing magnet. Principal quantum numbers up to about $n = 300$ can evade field ionization. On the average, Rydberg states with such high principal quantum numbers can easily survive the time of flight of the ions. An estimated fraction of about 0.02% of such ions in the parent ion beam would produce the observed background signal of 0.9 Mb at the ground-state ionization threshold energy of 818 eV. The background cross section increased towards lower electron energies reaching 1.3 Mb at 100 eV. The measurements taken at energies below the ground-state ionization potential were linearly extrapolated to 1000 eV and subtracted from the measured apparent cross section. Considering the small fraction of parent Rydberg ions producing the background cross section no correction for the primary ion current was required. The uncertainty of the extrapolation and background-subtraction procedure is substantial. It is estimated to be 25% of the resulting ground-state ionization cross section.

Nonsimultaneous measurement of parent ion current and ionization-signal rate is estimated to contribute to the total uncertainty with 5% of the corrected cross section. The statistical uncertainty of the corrected cross section at 1000 eV was also about 5%. From all the numbers provided, the quadrature sum of all uncertainties results in a total experimental uncertainty of 27% at an electron-ion collision energy of 1000 eV. Statistical uncertainties of the energy-scan data well above the ionization threshold are around 4%. The energy-scan data were normalized to the absolute data points by employing a linear correction function. The energy scale is determined to have an uncertainty of less than ± 1 eV. It has been corrected for possible contact-potential effects by comparison of the measured and expected ionization threshold of He^+ ions [58].

III. THEORY

Details of the theoretical method of calculating electron-impact excitation and multiple-ionization cross sections can be found in our recent work [40,59]. Therefore we only provide a short outline in the present context. The calculations were carried out by using the Flexible Atomic Code (FAC) developed by Gu [60]. A fine-structure level-to-level distorted-wave approximation is utilized to describe the electron excitation and ionization processes. A bound atomic state is constructed by a linear combination of configuration state functions (CSF), which are antisymmetric sums of the products of N one-electron Dirac spinors. The expansion coefficients of each CSF are determined by diagonalizing the relativistic Hamiltonian of the atomic system.

After obtaining the wave functions of the bound and continuum states, we can determine the electron-impact excitation (EIE) cross section,

$$\sigma_{\rm if} = \frac{2\pi}{k_i^2 g_i} \sum_{\kappa_i \kappa_f} \sum_{J_T} (2J_T + 1)|M|^2, \qquad (1)$$

with

$$|M|^2 = \left| \langle \psi_i \kappa_i, J_T M_T | \sum_{p<q} \frac{1}{r_{pq}} | \psi_f \kappa_f, J_T M_T \rangle \right|^2, \qquad (2)$$

where ψ_i and ψ_f are the wave functions of the initial and final states, respectively, g_i is the statistical weight of the initial state, and k_i is the kinetic momentum of the incident electron, κ_i and κ_f are the relativistic angular quantum numbers of the incident and scattered electrons, J_T is the total angular momentum when the target state is coupled to the continuum orbital, and M_T is the projection of the total angular momentum. The electron-impact ionization (EII) cross section can be obtained from an expression similar to that for EIE by replacing one bound orbital of the final state with the free orbital of the ejected electron.

The ground configuration of Zn-like Xe^{24+} is $[Ne]3s^2 3p^6 3d^{10} 4s^2$. The electron-impact ionization processes that contribute to net single ionization, i.e., the production of Xe^{25+}, are

$$e + 3s^2 3p^6 3d^{10} 4s^2 \rightarrow \begin{cases} 3s^2 3p^6 3d^{10} 4s + 2e \\ 3s^2 3p^6 3d^9 4s^2 + 2e \\ 3s^2 3p^5 3d^{10} 4s^2 + 2e \end{cases}. \qquad (3)$$

We do not include the ionization of a $3s$ electron as its ionization results in the production of the next higher ionization stage, Xe^{26+}, by Auger decay. For the same reason, removal of even more tightly bound K- and L-shell electrons is not considered either. Besides these direct-ionization processes (indirect, multistep), EA processes also contribute to the single-ionization cross section,

$$e + 3s^2 3p^6 3d^{10} 4s^2 \rightarrow \begin{cases} 3s^2 3p^6 3d^9 4s^2 nl + e \\ 3s^2 3p^5 3d^{10} 4s^2 nl + e. \\ 3s 3p^6 3d^{10} 4s^2 nl + e \end{cases} \qquad (4)$$

Here we do not include outermost-shell excitation to levels belonging to configurations $3s^2 3p^6 3d^{10} 4snl$ as these excited states are not autoionizing.

Compared with lower charge states of xenon ions, the contribution of REDA processes to electron-impact ionization of Xe^{24+} is relatively large and therefore has to be included in the total ionization cross section. The first step of REDA, resonant excitation also termed dielectronic capture, includes the following processes:

$$e + 3s^2 3p^6 3d^{10} 4s^2 \rightarrow \begin{cases} 3s^2 3p^6 3d^9 4s^2 nln'l' \\ 3s^2 3p^5 3d^{10} 4s^2 nln'l'. \\ 3s 3p^6 3d^{10} 4s^2 nln'l' \end{cases} \qquad (5)$$

The intermediate excited states can autoionize to form Xe^{25+} by releasing two electrons via two sequential Auger decays. We do not include the cross section for resonant excitation auto-double-ionization (READI) processes [2] as their contributions are negligibly small, which can be proven by employing our proposed simplified formalism for the description of direct-double Auger-decay processes [40,61,62]. Here we do not provide any details on calculations of these processes. For the same reason, the direct triple Auger decay processes have also been neglected although they can indeed happen [63].

According to the principle of detailed balance, the dielectronic capture (DC) cross section is obtained from the associated Auger decay rate,

$$\sigma_{ij}^{\mathrm{DC}}(E) = \frac{\pi^2\hbar^3}{m_e}\frac{g_j}{2g_i E_{ij}} A_{ji}^a S(E), \tag{6}$$

where i and j represent the initial levels of Xe^{24+} and the autoionizing excited levels of Xe^{23+}, respectively, E and E_{ij} are the incident-electron energy and the resonant energy, m_e is the rest mass of an electron, g_i and g_j are the statistical weights of states i and j, A_{ji}^a is the Auger rate from j to i, and $S(E)$ is the (Lorentzian) resonance line profile [40].

The total single-ionization cross section is obtained by summing the contributions from all possible processes discussed above,

$$\sigma = \sigma_d + \sum_i \sigma_i^{\mathrm{exc}} B_i^{1a} + \sum_k \sigma_k^{\mathrm{DC}} B_k^{2a}, \tag{7}$$

where σ_d, σ_i^{exc}, and σ_k^{DC} are the cross sections for direct ionization, for excitation to autoionizing intermediate levels i of the parent ion, and for dielectronic capture to intermediate levels k of the recombined ion, respectively. Branching ratios B_i^{1a} for single autoionization and B_k^{2a} for two sequential autoionization processes of the intermediate levels i and k describe the population of final levels within the bound-state spectrum of Xe^{25+}. Branching ratio for one-electron emission from an intermediate autoionizing level i can be written as

$$B_i^{1a} = \frac{\sum_l A_{il}^a}{\sum_m A_{im}^a + \sum_n A_{\mathrm{in}}^r}, \tag{8}$$

where the summation in the numerator extends over all nonautoionizing levels l of Xe^{25+}, while the summations in the denominator include all levels m of Xe^{25+} accessible by single autoionization of Xe^{24+} with the associated decay rates A_{im}^a and all levels n of Xe^{24+} accessible by radiative transitions $i \rightarrow n$ with the associated decay rates A_{in}^r.

The branching ratio for sequential emission of two electrons from an intermediate multiply excited level k of Xe^{23+} can then be formulated as

$$B_k^{2a} = \sum_{lf}\left(\frac{A_{kl}^a}{\sum_m A_{km}^a + \sum_n A_{kn}^r}\right)\left(\frac{A_{lf}^a}{\sum_m A_{lm}^a + \sum_n A_{ln}^r}\right), \tag{9}$$

where the summation over l comprises all intermediate autoionizing levels of Xe^{24+} while the summation over f includes, as mentioned before, all final levels belonging to the bound states of Xe^{25+}. The denominators are obtained by summing all decay rates of Xe^{23+} in level k and all decay rates of Xe^{24+} in level l, respectively.

IV. RESULTS AND DISCUSSIONS

We start with discussing the contributions of the DI and EA processes to the single-ionization cross section of Xe^{24+}. The results of the theoretical calculation for the ground state is shown by the solid line in Fig. 1(a). The calculations span an energy range from threshold to 4000 eV. The energy-axis label "incident electron energy" stands for electron-ion center-of-mass energy throughout the paper. For a quantitative understanding of the contributions from different processes, the DI cross sections of the $4s$, $3d$, and $3p$ subshells and the EA cross-section contributions of $3d$, $3p$, and $3s$ subshell excitations are given separately for comparison of their relative importance. The results show that EA processes dominate the ionization cross section over the whole energy range investigated. The largest contribution originates from $3d$ excitation. The calculated first ionization potential (IP) of Xe^{24+} is 818.2 eV, which is in good agreement with the National Institute of Standards and Technology (NIST) recommended value of 818 eV [58] (see Table I). This value resulted from systematic calculations [64] and has an estimated uncertainty of ±4 eV. There have been no measurements of the ionization potential of Xe^{24+} previously and the present measurement may provide the best experimental value, (818 ± 2) eV, available at this time.

The data in Table I suggest that the ionization of a $3d$ electron results in the production of Xe^{25+}, whereas a $3s$ vacancy must be expected to predominantly produce

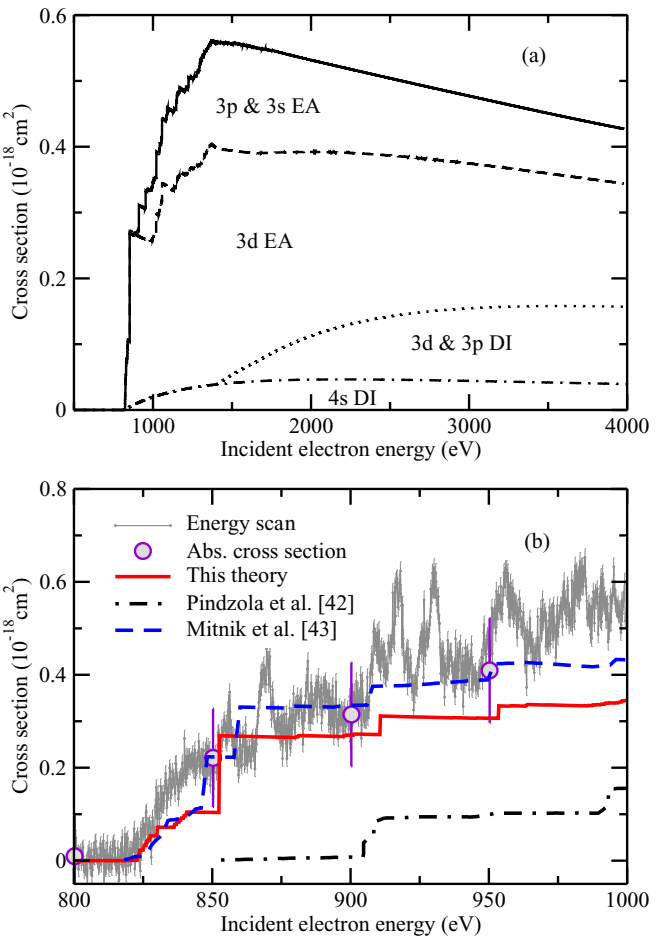

FIG. 1. (Color online) (a) Theoretical ionization cross section of Xe^{24+} (solid line) considering only contributions of DI and EA processes. The cross sections for DI of subshells $4s$, $3d$, and $3p$ and EA resulting from $3d$, $3p$, and $3s$ excitations are given separately. (b) Comparison between the theoretical and experimental cross sections from threshold to 1000 eV. The open points with relatively large error bars are the absolute experimental data. Theoretical results obtained previously by Pindzola *et al.* [42] and Mitnik *et al.* [43] are included.

TABLE I. Theoretical energies (in units of eV) of the energetically lowest levels within configurations of Xe^{24+}, Xe^{25+}, and Xe^{26+} relative to the ground level of Xe^{24+}. Completely filled subshells have been omitted to simplify the level designation.

Charge state	Level designation	Energy
Xe^{24+}	$(4s^2_{1/2})_0$	0.0
Xe^{25+}	$(4s_{1/2})_{1/2}$	818.2
Xe^{25+}	$(3d^{-1}_{5/2}4s^2_{1/2})_{5/2}$	1399.8
Xe^{25+}	$(3d^{-1}_{3/2}4s^2_{1/2}y)_{3/2}$	1413.3
Xe^{25+}	$(3p^{-1}_{3/2}4s^2_{1/2})_{3/2}$	1659.2
Xe^{25+}	$(3p^{-1}_{1/2}4s^2_{1/2})_{1/2}$	1724.1
Xe^{25+}	$(3s^{-1}_{1/2}4s^2_{1/2})_{1/2}$	1874.5
Xe^{26+}	$(3d^{10})_0$	1673.4

Xe^{26+} by multiple Auger decays as its energy lies above the double-ionization threshold of Xe^{24+} (1673.4 eV). When the $3p$ subshell is ionized, one fine-structure component $(3p^{-1}_{3/2}4s^2)$ leads to the production of Xe^{25+}, while the other $(3p^{-1}_{1/2}4s^2)$ can be expected to produce mainly Xe^{26+} by Auger decays. Calculations of the branching ratios verified the above expectations. The DI cross section denoted as "3d & 3p DI" in Fig. 1(a) is dominated by $3d$ ionization processes.

Electron-impact ionization cross sections of Xe^{24+} have been measured in the collision energy range from below the corresponding ground-state ionization threshold to 1000 eV. Theoretical and experimental cross sections are compared in Fig. 1(b). Previously available theoretical results obtained by Pindzola *et al.* [42] and Mitnik *et al.* [43] were restricted to the DI and EA contributions. They are shown along with the present experimental data and our present DI plus EA calculations.

Surprisingly, Pindzola *et al.* [42] who also used a distorted-wave approach predicted cross sections much below the present calculation (and experiment). Closer inspection shows that they falsely assumed the existence of an experimental ionization threshold of 852.6 eV (citing a previous version of the NIST reference data [58]) and therefore missed all the $3d \rightarrow 4f$ contributions to the ionization cross section. As mentioned above, there have been no experimental data for the ionization potential of Xe^{24+} previously. In such a case, the NIST recommended values are from (desirably the best) theoretical calculations. At some time in the past, the calculations by Carlson *et al.* [65] probably were the best available and their Xe^{24+} IP was 852.7 eV only one-tenth of an eV above what Pindzola *et al.* assumed to be an experimental threshold, but about 34 eV above the present results.

Mitnik *et al.* [43] predicted higher DI and EA cross section values than ours. One possible reason for the roughly 20% discrepancy is the different treatment of the electron correlation as was demonstrated in previous work [66–68]. From the comparison of the calculated results with the experimental data it becomes obvious that all theoretical calculations presented in Fig. 1(b) are missing an important cross-section contribution, namely, the resonances due to REDA processes which are clearly observed in the experiment.

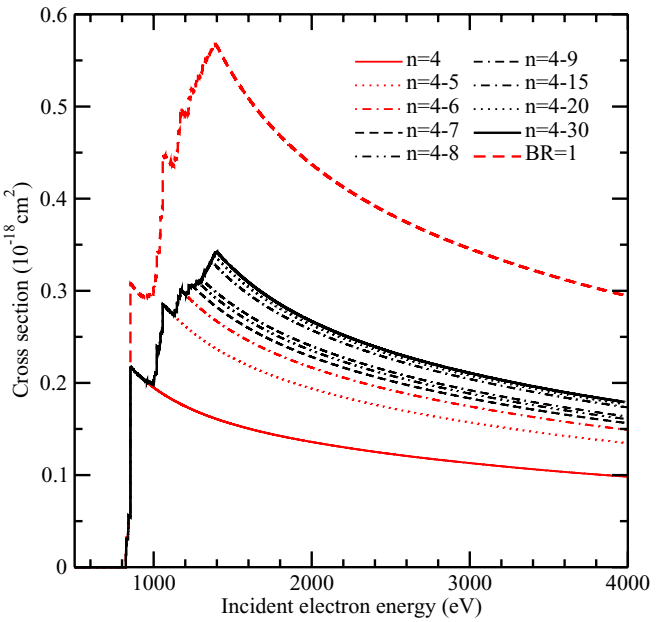

FIG. 2. (Color online) Convergence trend of cross sections for EA processes leading to $3s^23p^63d^94s^2nl$ intermediate configurations with principal quantum number n up to 30. For each n, contributions from all possible l have been included. The dashed (red) line represents the total EA cross section assuming the branching ratios to be unity (BR = 1).

There are so many resonances that they enhance the continuum DI- and EA-based cross section by more than 0.15 Mb in the incident-electron energy range of 950–1000 eV, i.e., by about 50% compared with our theoretical result. At lower energies there are resonance structures enhancing the total single-ionization cross section by almost 100% beyond the calculated DI and EA contributions.

For obtaining the theoretical results shown in Fig. 1(b), the EA processes have been calculated up to very high nl (with the principal quantum number n up to 30 and accounting for all possible l values for each n). Figure 2 shows the convergence trend of $3d \rightarrow nl$ EA processes with $3s^23p^63d^94s^2nl$ intermediate configurations. The results show that nl up to $n = 15$ or even $n = 20$ should be included for Xe^{24+}. The necessity for including such high nl configurations in the calculation for Xe^{24+} is different from findings for ions in lower charge states [24,40]. Our conclusion that higher charge states require inclusion of higher nl states is in agreement with recent work by Jonauskas *et al.* [69]. They investigated the effects of high-nl EA contributions to the electron-impact ionization of W^{27+} by performing relativistic subconfiguration-average and detailed level-to-level calculations illustrating the role of high shells ($n \geqslant 9$) and their influence on the total ionization cross section.

Another feature in the electron-impact ionization of Xe^{24+} is that branching ratios play a more important role than for the lower charge states of ions along the xenon iso-nuclear sequence. By assuming unity branching ratios (BR=1), we get the result represented by the (red) dashed line in Fig. 2. Large differences are found between the EA cross sections with and without considering the branching ratios.

TABLE II. Energy (eV), sum of Auger rates (s^{-1}), sum of radiative rates (s^{-1}), and branching ratios (BR) of some of the dominating EA channels. The energy is relative to that of the ground level of Xe^{24+}. Numbers in square brackets in the second and third columns indicate powers of ten.

EA intermediate level	Energy	Auger rate	Radiative rate	BR
$3s^23p^6(3d^9_{5/2}4s^24f_{7/2})_1$	830.1	9.722[12]	5.306[12]	0.647
$3s^23p^6(3d^9_{3/2}4s^24f_{5/2})_1$	852.3	1.057[14]	5.850[13]	0.644
$3s^2(3p^5_{3/2}3d^{10}4s^24p_{3/2})_0$	910.5	3.487[14]	2.231[12]	0.994
$3s^23p^6(3d^9_{5/2}4s^25p_{1/2})_3$	949.8	1.566[11]	5.012[11]	0.238
$3s^23p^6(3d^9_{3/2}4s^25d_{3/2})_0$	949.8	4.213[14]	5.813[11]	0.999

The cross sections obtained by assuming BR=1 are too high by about 64% for incident electron energies from 1200 eV to 4000 eV. At the same time it is evident that different EA channels involve different branching ratios. In Table II we list several strong EA channels characterized by their intermediate autoionizing levels. These channels provide relatively large contributions to the cross section. For EA via $3s^23p^63d^94s^2nf$ states the dominating channels are $3s^23p^6(3d^9_{5/2}4s^2nf_{7/2})_1$ and $3s^23p^6(3d^9_{3/2}4s^2nf_{5/2})_1$. For $n=4$, we predict BR=0.647 and BR=0.644, respectively. For $3s^23p^53d^{10}4s^2np$ intermediate configurations, the dominating channel is $3s^2(3p^5_{3/2}3d^{10}4s^2np_{3/2})_0$ with a BR=0.994 for $n=4$ while a much smaller BR=0.238 is found for the most important channel via the $3s^23p^63d^94s^25p$ configuration. The main EA channels with excitation of levels within the $3s^23p^63d^94s^2nd$ Rydberg series are also listed in Table II. From the above discussion it becomes obvious that the branching ratios play an important role in the determination of EA cross sections. The role of the dominating channels contributing to electron-impact ionization of Xe^{24+} can be inferred from Fig. 3. In order to aid the understanding, the total EA cross section is shown as a dotted line. It can be seen that the five channels listed in Table II indeed provide the dominating EA contribution near the ionization threshold.

From the comparison shown in Fig. 1(b), we see that theoretical calculations including only DI and EA processes cannot explain the experiment. Obviously, REDA processes play an important role in electron-impact ionization of Xe^{24+} ions. There is a new quality of REDA features here as compared to lower ionization stages. For the low and moderate charge states q of Xe^{q+} ions [24–26] one can neglect cross-section contributions via dielectronic capture [2] to levels with very high principal and orbital angular-momentum quantum numbers n' ($n' > 10$) and l' ($l' > 5$), respectively. For Xe^{24+}, however, one has to include these higher $n'l'$ contributions to obtain accurate results. As an example, Fig. 4 shows the cross-section contributions of REDA channels proceeding via resonant excitation to $3s^23p^63d^94s^25f9l'$ with $l' = 0,1,...,8$ respectively. The resonances are represented as Voigt profiles which resulted from convolution of the original Lorentzian profiles with Gaussians of 2 eV half width at half maximum (HWHM). The instrumental resolving power was not determined in the present experiment, however, previous estimates of the energy spread of the electron beam at energies

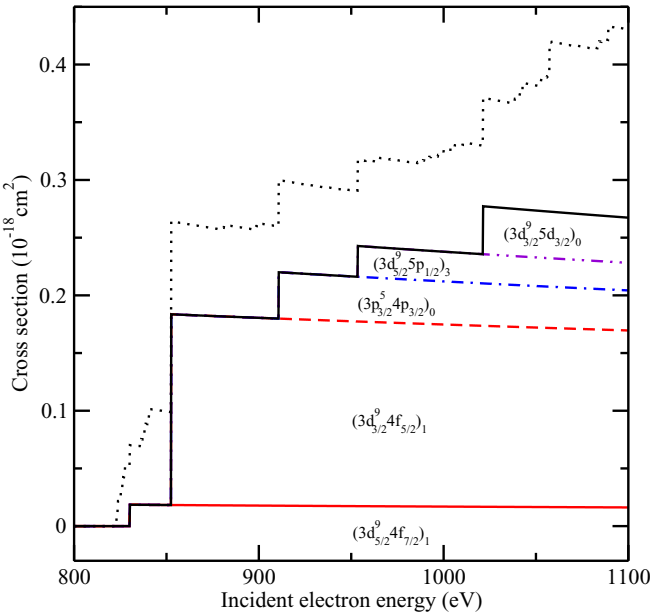

FIG. 3. (Color online) The cross-section contributions of the five EA channels listed in Table II. The total EA cross section represented by the dotted line is shown for comparison.

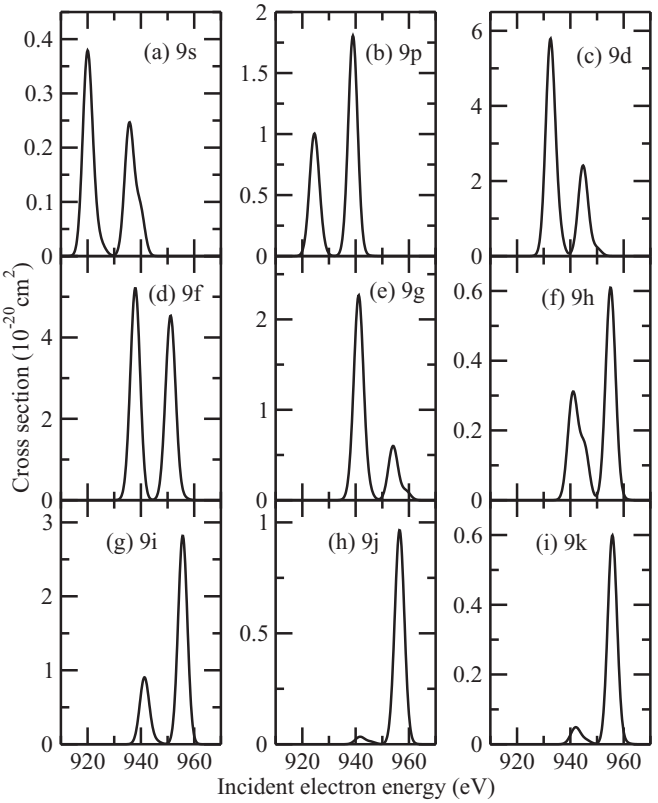

FIG. 4. Cross sections of REDA channels proceeding via resonant excitation of $Xe^{24+}(3s^23p^63d^{10}4s^2)$ to $Xe^{23+}(3s^23p^63d^94s^25f9l')$ with $l' = 0,1,...,8$, respectively, showing the relatively strong contributions of excitations to all subshells characterized by l'.

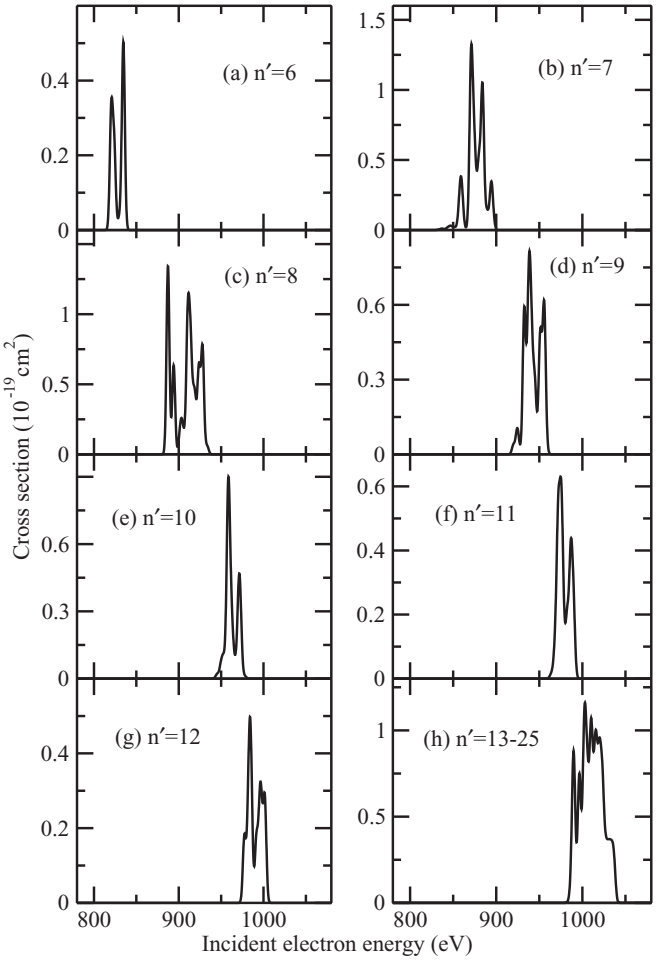

FIG. 5. Slow convergence of the cross sections for REDA processes involving $3s^23p^63d^94s^25fn'l'$ configurations with the principal quantum number n'. For each n', contributions of all possible l' are considered.

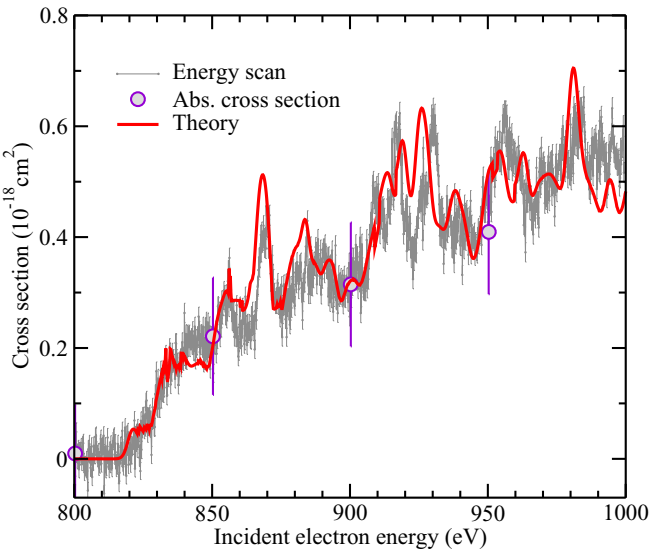

FIG. 6. (Color online) Comparison between the theoretical and experimental ionization cross section of Xe^{24+}. The experimental data are the same as those shown in Fig. 1.

beyond 800 eV are compatible with or slightly better than 4 eV [70,71].

Inspection of Fig. 4 shows that the dominant REDA contributions originate from $3s^23p^63d^94s^25f9d$ and $3s^23p^63d^94s^25f9f$ resonances. Yet, even the cross sections associated with the highest l' quantum numbers of the resonant configurations $3s^23p^63d^94s^25f9l'$, with $l' = 6,7,8$ corresponding to i,j,k may not be neglected. For higher n' a similar conclusion still holds. As a result, one should include all possible l' ($l' = 0,1,...,n-1$) for a given n'. Moreover, the convergence of REDA contributions with n' is also slow and one has to include REDA contributions up to very high n'. In Fig. 5 an example is provided for the REDA processes via $Xe^{23+}(3s^23p^63d^94s^25fn'l')$ configurations. For each principal quantum number n' the calculated REDA spectra include all contributions from all subshells characterized by their orbital angular-momentum quantum number l'. In the figure, the resonance group labeled with $n' = 6$, for example, is associated with configurations $3s^23p^63d^94s^25f6l'$ and includes all contributions with $l' = 0,1,...,5$. The largest REDA contributions originate from $3s^23p^63d^94s^25f7l'$ and $3s^23p^63d^94s^25f8l'$ configurations, yet resonances with higher n' cannot be neglected. Furthermore, the contribution from higher n' tends to form a quasicontinuum band. The fact of the slow convergence of REDA with n' and l' increases the difficulty of calculating REDA contributions to the total single-ionization cross section for highly charged ions.

After adding all the REDA contributions to the DI and EA cross sections, the total theoretical electron-impact single-ionization cross section is obtained. This is compared in Fig. 6 with the present experimental results. Good agreement is found between theory and experiment. To obtain such an agreement, we have to calculate and include contributions from high principal quantum numbers n' up to 25 in the theoretical cross section. However, in some cases, for particular core-excitation channels, even REDA contributions with higher n' were required to be included. Take the series of $3s^23p^63d^94s^24fn'l'$ as an example to illustrate this issue. The Xe^{23+} levels belonging to configurations $3s^23p^63d^94s^24fn'l'$ with $n' < 27$ cannot decay to Xe^{25+}, i.e., their BR = 0. However, levels with higher n' ($\geqslant 27$) can emit two electrons sequentially and thus decay to Xe^{25+}. In a first guess one would expect that the contributions from such high n' ($\geqslant 27$) should be small and might be negligible. And yet these channels have to be included to obtain a better agreement with the experimental result. Thus, in this work, the maximum n' for which calculations were performed reached $n' = 39$ for that particular Rydberg series associated with $3d \rightarrow 4f$ core excitations. The contributions from $3s^23p^63d^94s^24fn'l'$ ($27 \leqslant n' \leqslant 39$) are located in the incident-electron energy range of 830–850 eV.

V. CONCLUSION

In conclusion, electron-impact ionization cross sections of the ground state of Xe^{24+} have been investigated experimentally and theoretically. The experimental cross section shows rich resonance structures from threshold up to 1000 eV. Detailed level-to-level distorted-wave calculations were carried

out to study the respective contributions from direct ionization (DI), excitation-autoionization (EA), and resonant-excitation double-autoionization (REDA) processes. The dominating EA channels and the corresponding branching ratios have been determined. EA and REDA processes dominate the total single-ionization cross section. To accurately determine their contributions, one has to consider processes of very-high-nl subshells of intermediate multiply excited states, especially for the REDA channels. The slow convergence of REDA cross sections of resonances with the principal quantum number n' and orbital angular-momentum quantum number l' of the recombined electron requires calculations for sufficiently large $n'l'$ to be included. Only then good agreement with the experiment can be obtained. The present study and its results should be helpful for the further investigation of electron-ion collision processes of highly charged ions and particularly for the isonuclear sequences of xenon, tin, and tungsten, which have wide applications in various research fields such as ultraviolet lithography and magnetic confinement fusion.

ACKNOWLEDGMENTS

This work was supported by the National Natural Science Foundation of China under Grant No. 11274382. Support by Deutsche Forschungsgemeinschaft (DFG) through Grants No. Mu-1068/14 and No. Mu-1068/20 is gratefully acknowledged.

[1] T. R. Kallman and P. Palmeri, Rev. Mod. Phys. **79**, 79 (2007).
[2] A. Müller, Adv. At. Mol. Opt. Phys. **55**, 293 (2008).
[3] E. Landi and M. Landini, Astron. Astrophys. **347**, 401 (1999).
[4] P. Bryans, E. Landi, and D. W. Savin, Astrophys. J. **691**, 1540 (2009).
[5] A. Müller, E. Salzborn, R. Frodl, R. Becker, H. Klein, and H. Winter, J. Phys. B **13**, 1877 (1980).
[6] C. Achenbach, A. Müller, E. Salzborn, and R. Becker, Phys. Rev. Lett. **50**, 2070 (1983).
[7] D. C. Gregory and D. H. Crandall, Phys. Rev. A **27**, 2338 (1983).
[8] D. C. Gregory, P. F. Dittner, and D. H. Crandall, Phys. Rev. A **27**, 724 (1983).
[9] C. Achenbach, A. Müller, E. Salzborn, and R. Becker, J. Phys. B **17**, 1405 (1984).
[10] A. Müller, C. Achenbach, E. Salzborn, and R. Becker, J. Phys. B **17**, 1427 (1984).
[11] M. S. Pindzola, D. C. Griffin, C. Bottcher, D. H. Crandall, R. A. Phaneuf, and D. C. Gregory, Phys. Rev. A **29**, 1749 (1984).
[12] D. C. Griffin, C. Bottcher, M. S. Pindzola, S. M. Younger, D. C. Gregory, and D. H. Crandall, Phys. Rev. A **29**, 1729 (1984).
[13] A. Danjo, A. Matsumoto, S. Ohtani, H. Suzuki, H. Tawara, K. Wakiya, and M. Yoshino, J. Phys. Soc. Jpn. **53**, 4091 (1984).
[14] A. M. Howald, D. C. Gregory, R. A. Phaneuf, D. H. Crandall, and M. S. Pindzola, Phys. Rev. Lett. **56**, 1675 (1986).
[15] K. F. Man, A. C. H. Smith, and M. F. A. Harrison, J. Phys. B **20**, 5865 (1987).
[16] M. E. Bannister, D. W. Mueller, L. J. Wang, M. S. Pindzola, D. C. Griffin, and D. C. Gregory, Phys. Rev. A **38**, 38 (1988).
[17] D. W. Mueller, L. J. Wang, and D. C. Gregory, Phys. Rev. A **39**, 2381 (1989).
[18] A. Matsumoto, A. Danjo, S. Ohtani, H. Suzuki, H. Tawara, T. Takayanagi, K. Wakiya, I. Yamada, M. Yoshino, and T. Hirayama, J. Phys. Soc. Jpn. **59**, 902 (1990).
[19] E. W. Bell, N. Djurić, and G. H. Dunn, Phys. Rev. A **48**, 4286 (1993).
[20] K. F. Man, A. C. H. Smith, and M. F. A. Harrison, J. Phys. B **26**, 1365 (1993).
[21] G. Hofmann, J. Neumann, U. Pracht, K. Tinschert, M. Stenke, R. Völpel, A. Müller, and E. Salzborn, in *The Physics of Highly Charged Ions*, edited by P. R. M. Stöckli, C. L. Cocke, and C. D. Lin, AIP Conf. Proc., No. 274 (AIP, College Park, 1993), p. 485.
[22] M. Stenke, K. Aichele, D. Hathiramani, G. Hofmann, M. Steidl, R. Völpel, and E. Salzborn, Nucl. Instrum. Methods B **98**, 573 (1995).
[23] E. D. Emmons, A. Aguilar, M. F. Gharaibeh, S. W. J. Scully, R. A. Phaneuf, A. L. D. Kilcoyne, A. S. Schlachter, I. Alvarez, C. Cisneros, and G. Hinojosa, Phys. Rev. A **71**, 042704 (2005).
[24] A. Borovik Jr., C. Brandau, J. Jacobi, S. Schippers, and A. Müller, J. Phys. B **44**, 205205 (2011).
[25] M. S. Pindzola, S. D. Loch, A. Borovik Jr., M. F. Gharaibeh, J. K. Rudolph, S. Schippers, and A. Müller, J. Phys. B **46**, 215202 (2013).
[26] A. Borovik Jr., M. F. Gharaibeh, S. Schippers, and A. Müller, J. Phys. B **48**, 035203 (2015).
[27] A. Borovik Jr., J. Rausch, J. Rudolph, M. Gharaibeh, S. Schippers, and A. Müller, J. Phys. Conf. Ser. **194**, 062014 (2009).
[28] D. Schneider, D. DeWitt, M. W. Clark, R. Schuch, C. L. Cocke, R. Schmieder, K. J. Reed, M. H. Chen, R. E. Marrs, M. Levine, and R. Fortner, Phys. Rev. A **42**, 3889 (1990).
[29] K. J. LaGattuta and Y. Hahn, Phys. Rev. A **24**, 2273 (1981).
[30] A. Müller, K. Tinschert, G. Hofmann, E. Salzborn, and G. H. Dunn, Phys. Rev. Lett. **61**, 70 (1988).
[31] A. Müller, G. Hofmann, K. Tinschert, and E. Salzborn, Phys. Rev. Lett. **61**, 1352 (1988).
[32] D. L. Moores and K. J. Reed, Adv. At. Mol. Phys. **34**, 301 (1994).
[33] J. Kenntner, J. Linkemann, N. R. Badnell, C. Broude, D. Habs, G. Hofmann, A. Müller, M. S. Pindzola, E. Salzborn, D. Schwalm, and A. Wolf, Nucl. Instrum. Methods B **98**, 142 (1995).
[34] H. Teng, H. Knopp, S. Ricz, S. Schippers, K. A. Berrington, and A. Müller, Phys. Rev. A **61**, 060704 (2000).
[35] A. Müller, H. Teng, G. Hofmann, R. A. Phaneuf, and E. Salzborn, Phys. Rev. A **62**, 062720 (2000).
[36] J. Linkemann, A. Müller, J. Kenntner, D. Habs, D. Schwalm, A. Wolf, N. R. Badnell, and M. S. Pindzola, Phys. Rev. Lett. **74**, 4173 (1995).
[37] J. Linkemann, J. Kenntner, A. Müller, A. Wolf, D. Habs, D. Schwalm, W. Spies, O. Uwira, A. Frank, A. Liedtke, G. Hofmann, E. Salzborn, N. R. Badnell, and M. S. Pindzola, Nucl. Instrum. Methods B **98**, 154 (1995).
[38] H. Teng, J. Phys. B **33**, L553 (2000).

[39] A. Müller, A. Borovik Jr., K. Huber, S. Schippers, D. V. Fursa, and I. Bray, Phys. Rev. A **90**, 010701(R) (2014).
[40] P. F. Liu, Y. P. Liu, J. L. Zeng, and J. M. Yuan, Phys. Rev. A **89**, 042704 (2014).
[41] A. Borovik Jr., M. F. Gharaibeh, P. M. Hillenbrand, S. Schippers, and A. Müller, J. Phys. B **46**, 175201 (2013).
[42] M. S. Pindzola, C. P. Ballance, J. A. Ludlow, S. D. Loch, and D. C. Griffin, J. Phys. B **43**, 025201 (2010).
[43] D. Mitnik, P. Mandelbaum, J. L. Schwob, A. Bar-Shalom, and J. Oreg, Phys. Rev. A **55**, 307 (1997).
[44] P. H. Norrington and I. P. Grant, J. Phys. B **20**, 4869 (1987).
[45] P. Defrance, F. Brouillard, W. Claeys, and G. Van Wassenhove, J. Phys. B **14**, 103 (1981).
[46] A. Müller, K. Huber, K. Tinschert, R. Becker, and E. Salzborn, J. Phys. B **18**, 2993 (1985).
[47] A. Müller, K. Tinschert, C. Achenbach, R. Becker, and E. Salzborn, Nucl. Instrum. Methods B **10**, 204 (1985).
[48] A. Müller, G. Hofmann, B. Weissbecker, M. Stenke, K. Tinschert, M. Wagner, and E. Salzborn, Phys. Rev. Lett. **63**, 758 (1989).
[49] J. Jacobi, H. Knopp, S. Schippers, A. Müller, S. D. Loch, M. Witthoeft, M. S. Pindzola, and C. P. Ballance, Phys. Rev. A **70**, 042717 (2004).
[50] A. Borovik Jr., A. Müller, S. Schippers, I. Bray, and D. V. Fursa, J. Phys. B **42**, 025203 (2009).
[51] R. Trassl, W. R. Thompson, F. Broetz, M. Pawlowsky, R. W. McCullough, and E. Salzborn, Phys. Scr. **T80B**, 504 (1999).
[52] R. Becker, A. Müller, C. Achenbach, K. Tinschert, and E. Salzborn, Nucl. Instrum. Methods B **9**, 385 (1985).
[53] W. Shi, J. Jacobi, H. Knopp, S. Schippers, and A. Müller, Nucl. Instrum. Methods B **205**, 201 (2003).
[54] A. Borovik Jr., W. Shi, J. Jacobi, S. Schippers, and A. Müller, J. Phys.: Conf. Ser. **488**, 142007 (2014).
[55] J. Fricke, A. Müller, and E. Salzborn, Nucl. Instrum. Methods **175**, 379 (1980).
[56] K. Rinn, A. Müller, H. Eichenauer, and E. Salzborn, Rev. Sci. Instrum. **53**, 829 (1982).
[57] J. Rausch, A. Becker, K. Spruck, J. Hellhund, A. Borovik Jr., K. Huber, S. Schippers, and A. Müller, J. Phys. B **44**, 165202 (2011).
[58] A. E. Kramida, Yu. Ralchenko, J. Reader, and NIST ASD Team (2014), *NIST Atomic Spectra Database (Version 5.2)* (National Institute of Standards and Technology, Gaithersburg, 2014), available online: http://physics.nist.gov/asd.
[59] J. L. Zeng, L. P. Liu, P. F. Liu, and J. M. Yuan, Phys. Rev. A **90**, 044701 (2014).
[60] M. F. Gu, Can. J. Phys. **86**, 675 (2008).
[61] J. L. Zeng, P. F. Liu, W. J. Xiang, and J. M. Yuan, Phys. Rev. A **87**, 033419 (2013).
[62] J. L. Zeng, P. F. Liu, W. J. Xiang, and J. M. Yuan, J. Phys. B **46**, 215002 (2013).
[63] A. Müller, A. Borovik Jr., T. Buhr, J. Hellhund, K. Holste, A. L. D. Kilcoyne, S. Klumpp, M. Martins, S. Ricz, J. Viefhaus, and S. Schippers, Phys. Rev. Lett. **114**, 013002 (2015).
[64] G. C. Rodrigues, P. Indelicato, J. P. Santos, P. Patté, and F. Parente, At. Data Nucl. Data Tables **86**, 117 (2004).
[65] T. A. Carlson, C. W. Nestor, N. Wassermann, and J. D. McDowell, Atomic Data **2**, 63 (1970).
[66] J. L. Zeng and J. M. Yuan, Phys. Rev. E **74**, 025401(R) (2006).
[67] J. Zeng and J. Yuan, Phys. Rev. E **76**, 026401 (2007).
[68] J. Zeng, J. Phys. B **41**, 125702 (2008).
[69] V. Jonauskas, A. Kynienė, G. Merkelis, G. Gaigalas, R. Kisielius, S. Kučas, Š. Masys, L. Radžiūtė, and P. Rynkun, Phys. Rev. A **91**, 012715 (2015).
[70] K. Aichele, W. Shi, F. Scheuermann, H. Teng, E. Salzborn, and A. Müller, Phys. Rev. A **63**, 014701 (2000).
[71] K. Aichele, D. Hathiramani, F. Scheuermann, A. Müller, E. Salzborn, D. Mitnik, J. Colgan, and M. S. Pindzola, Phys. Rev. Lett. **86**, 620 (2001).